Supplementary materials

Table S1 Effect of retention time on the dissolution of main impurity metals mg/L

Time/h	Ca	Al	Fe	Cu
1.0	2.16	8.31	0.80	10.29
1.5	4.02	13.39	9.17	15.35
2.0	6.18	26.17	28.68	30.72
2.5	8.53	33.34	41.97	37.45
3.0	9.60	36.97	56.41	36.08
3.5	10.22	31.68	60.23	34.98
4.0	9.93	34.21	58.56	40.04

Table S2 Effect of temperature on the dissolution of main impurity metals mg/L

T/°C	Ca	Al	Fe	Cu
50	1.02	4.28	4.39	1.07
60	2.29	7.63	9.57	3.14
70	3.67	12.26	17.10	8.69
80	5.25	21.33	34.99	16.77
90	9.60	36.97	56.42	36.11
100	10.11	35.71	57.12	33.59
110	9.97	36.15	58.30	38.30
120	10.06	34.58	60.29	35.04

Table S3 Effect of ligand concentration on the dissolution of main impurity metals mg/L

$[Gly^-]_T$/(mol·L^{-1})	Ca	Al	Fe	Cu
0.5	0.86	1.96	1.60	2.01
1.0	1.13	3.15	3.47	4.14
1.5	1.44	4.58	3.95	6.72
2.0	2.20	8.33	7.55	6.46
2.5	3.08	10.82	11.39	8.56
3.0	3.67	12.26	17.10	8.69
3.5	3.97	10.11	18.30	8.01
4.0	3.88	11.58	18.75	8.95
4.5	4.01	10.76	19.16	8.62
5.0	3.77	11.52	19.22	8.17

Table S4 Effect of liquid-solid ratio on the dissolution of main impurity metals mg/L

(L/S)/(mL:g)	Ca	Al	Fe	Cu
3:1	8.15	29.25	47.38	29.85
4:1	7.66	31.25	45.06	34.95
5:1	9.60	36.97	56.41	36.08
6:1	9.79	36.21	56.81	36.45
7:1	8.36	40.33	54.04	39.08
8:1	6.53	41.78	57.55	36.45
9:1	8.22	42.44	58.12	37.12
10:1	7.36	42.53	53.13	34.13
11:1	8.58	43.68	57.74	29.40
15:1	9.13	45.07	48.96	27.68
20:1	9.14	44.79	50.30	26.31

Table S5 Effect of pH on the dissolution of main impurity metals mg/L

pH	Ca	Al	Fe	Cu
6.0	11.23	41.81	59.66	39.52
7.0	11.57	41.76	60.08	35.15
8.0	9.60	36.97	56.41	36.08
9.0	8.01	29.98	54.93	31.23
10.0	5.45	20.31	43.22	23.86
11.0	6.11	8.12	39.71	15.89
12.0	5.77	2.76	37.15	16.08

Table S6 Effect of stirring speed on the dissolution of main impurity metals mg/L

n/(r·min^{-1})	Ca	Al	Fe	Cu
200	9.09	29.40	48.59	33.55
300	8.97	34.23	50.25	32.72
400	9.60	36.97	56.41	36.08
500	10.22	39.86	57.46	36.48
600	10.06	34.53	55.18	34.02

Table S7 Effect of hydrogen peroxide (30%) volume ratio on the dissolution of main impurity metals mg/L

Volume ratio/%	Ca	Al	Fe	Cu
0	9.60	36.97	56.41	36.08
2	11.73	39.95	53.24	39.27
5	13.52	46.13	53.56	40.04
8	14.65	43.50	54.83	39.84
10	10.94	45.61	56.41	36.92

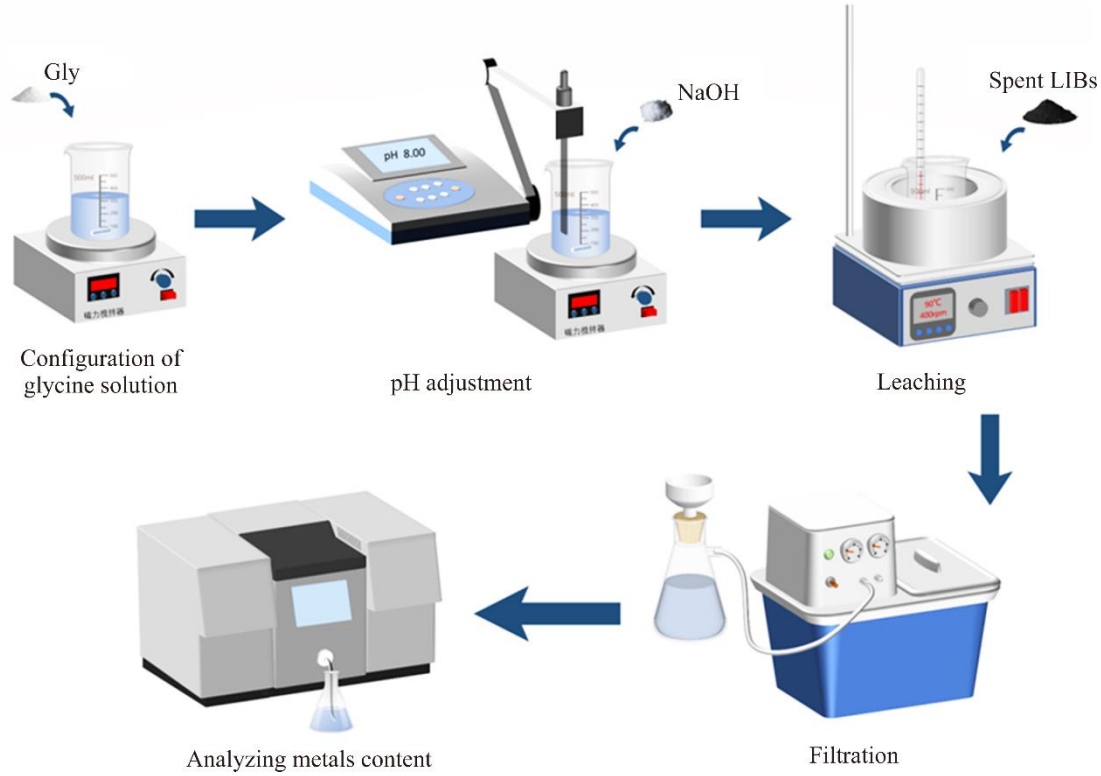

Figure S1 Reaction flow chart

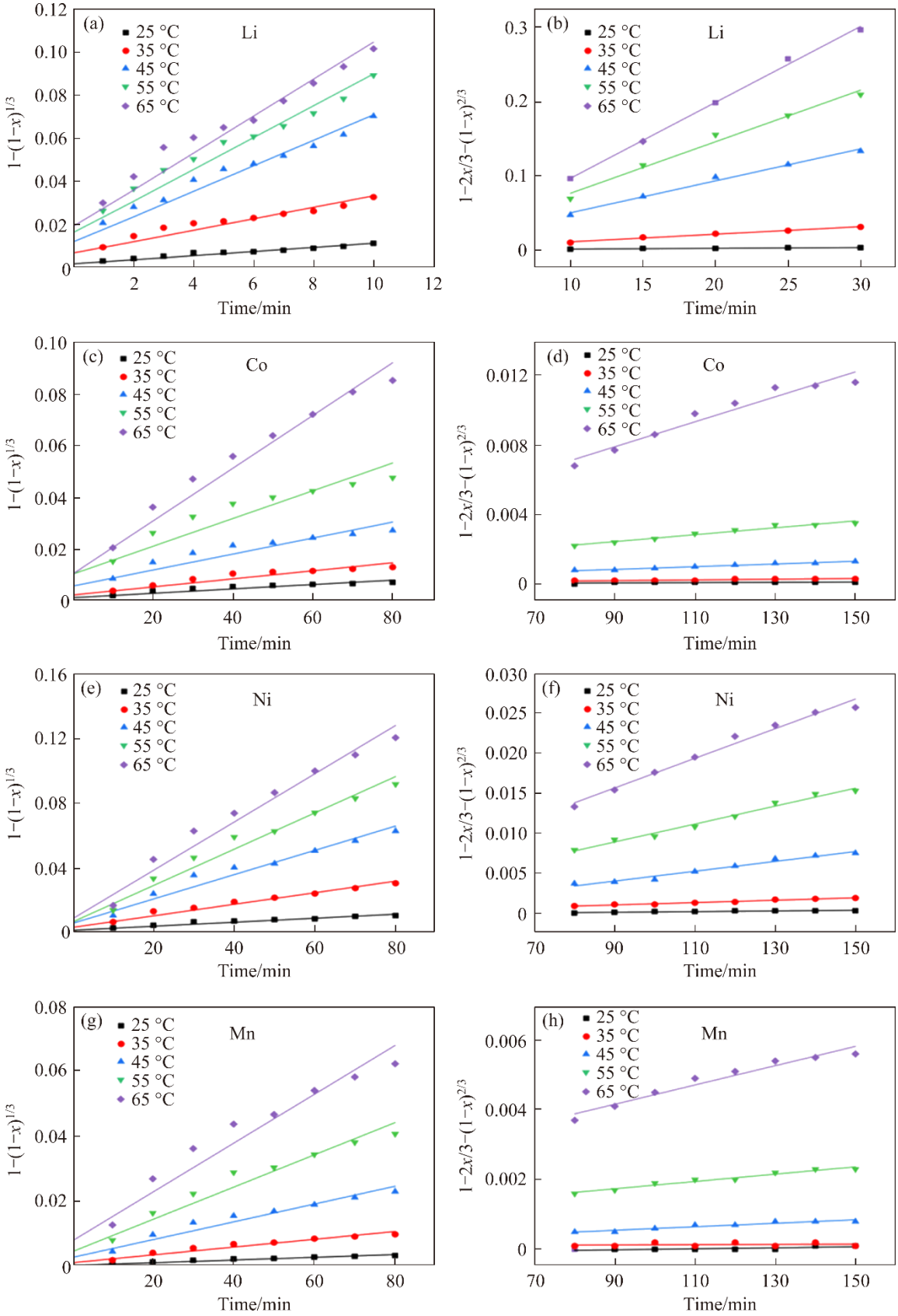

Figure S2 Variation of $1-(1-x)^{1/3}$ with time of leaching Li, Co, Ni and Mn at different temperatures (a, c, e, g); Variation of $1-2x/3-(1-x)^{2/3}$ with time of leaching Li, Co, Ni, and Mn at different temperatures(b, d, f, h)

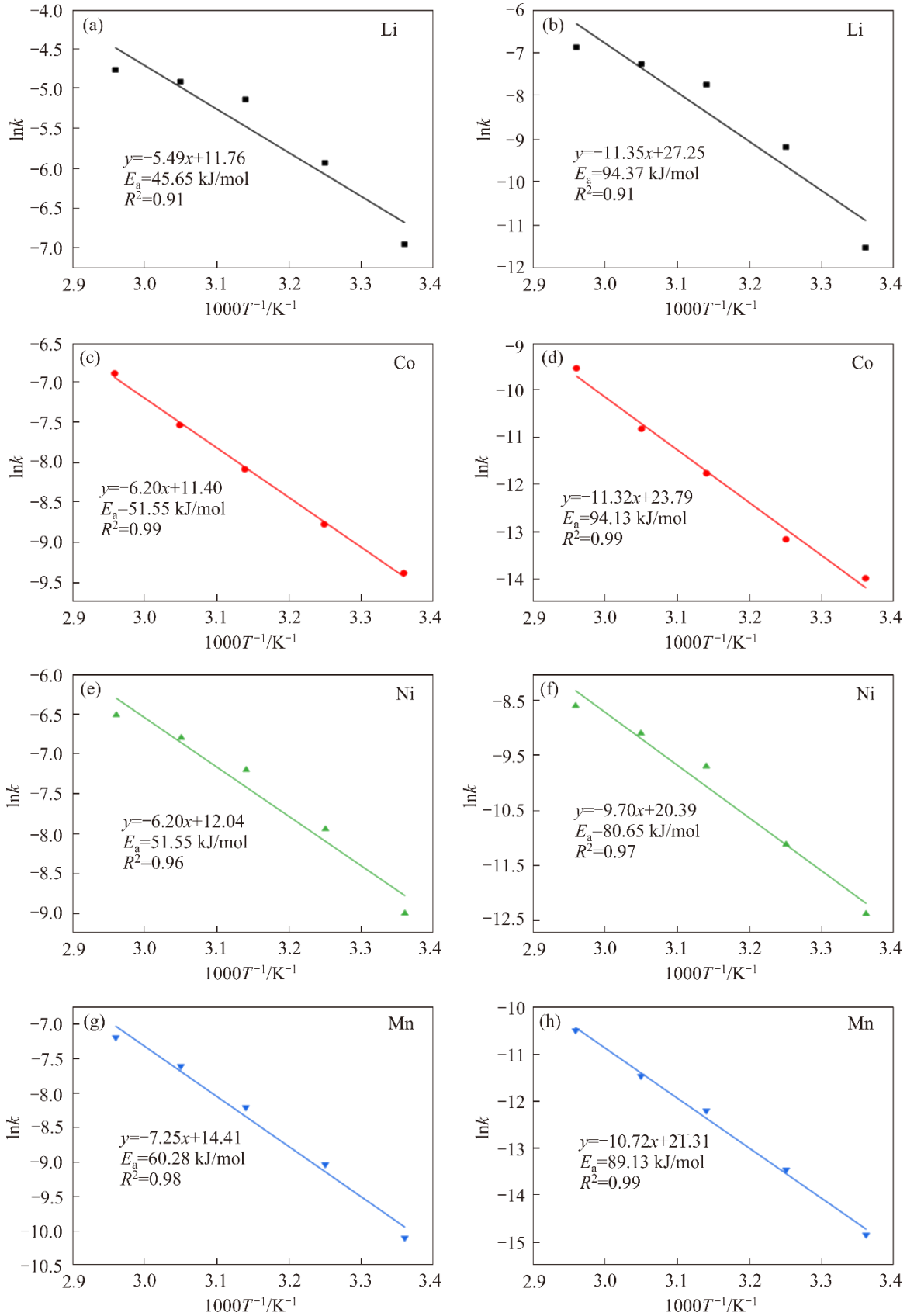

Figure S3 Arrhenius curves of Li, Co, Ni, and Mn in the temperature range 298−338 K

The correlation results of the second-step activation energy fit are shown in Figure S3. The leaching activation energies of Li, Ni, Co and Mn are 94.37, 94.13, 80.65 and 89.13 kJ/mol, respectively. The activation energies of Li, Co, Ni and Mn all exceed 42 kJ/mol, which is not consistent with the activation energy

controlled by the internal diffusion reaction, indicating that the leaching reaction is not controlled by the internal diffusion reaction in this section.

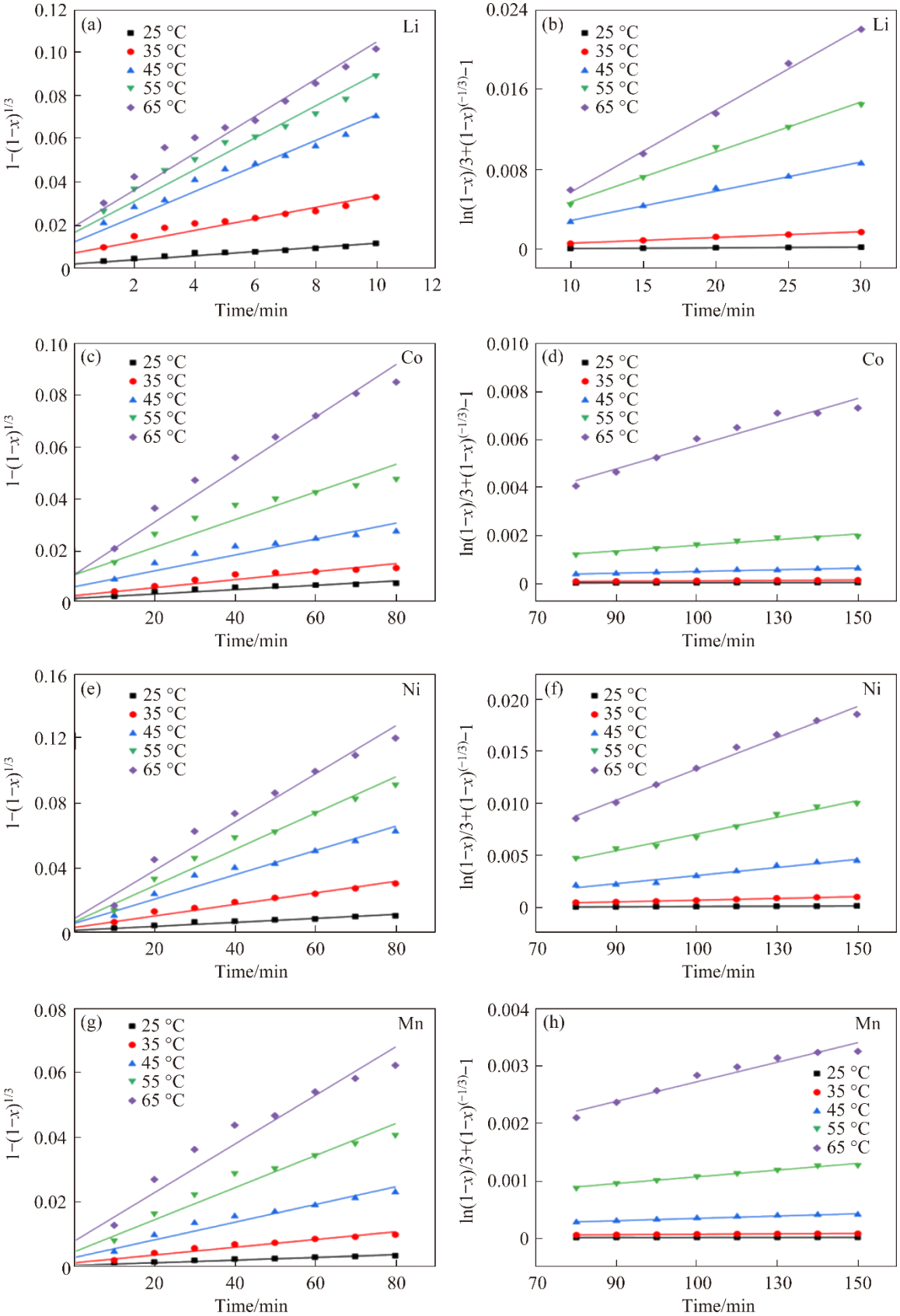

Figure S4 Variation of $1-(1-x)^{1/3}$ with a time of leaching Li, Co, Ni and Mn at different temperatures (a, c, e, g); Variation of $\ln(1-x)/3+(1-x)^{(-1/3)}-1$ with a time of leaching Li, Co, Ni and Mn at different temperatures(b, d, f, h)

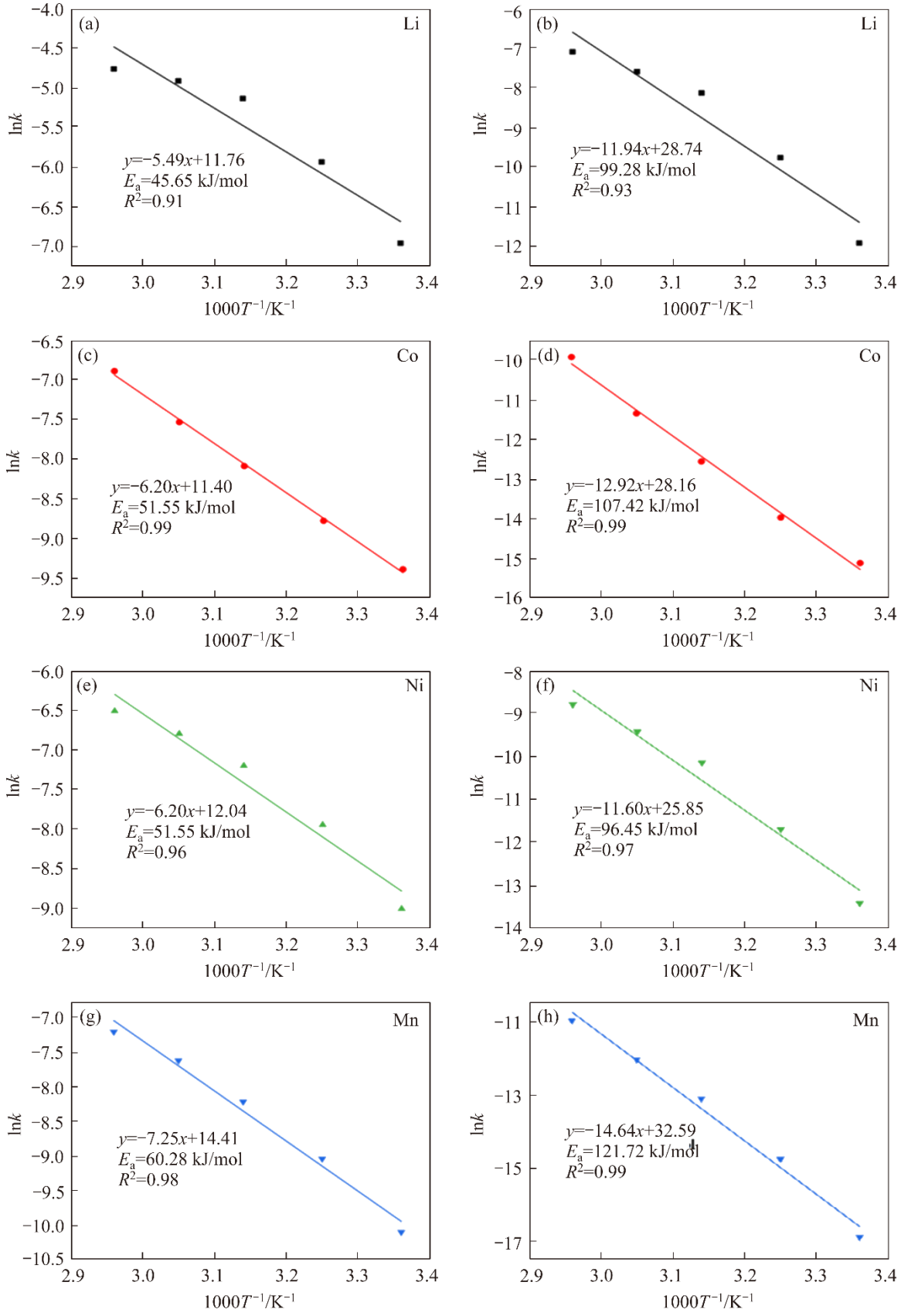

Figure S5 Arrhenius curves of Li, Co, Ni and Mn in the temperature range 25−65 °C

In the second paragraph, the activation energies (E_a) of Li, Co, Ni and Mn in the mixed reaction control were calculated according to the Arrhenius equation as 99.28, 107.42, 96.45 and 121.72 kJ/mol, respectively.

The activation energies of Li, Co, Ni and Mn were much more than 42 kJ/mol, which is not in line with the activation energy controlled by the mixed reaction, indicating that the leaching reaction is not controlled by the mixed reaction. Therefore, the kinetic analysis of the dissolution of valent metal elements in decommissioned lithium-ion batteries in the alkaline glycinate system is not suitable to be divided into two-step control methods.

After leaching the spent LIBs powder through an alkaline glycinate system and obtaining a relatively pure leaching solution containing Li, Co, Ni and Mn, a new NCM111 precursor was synthesized by a hydroxide co-precipitation preparation process. Then, NCM111 anode materials were prepared by mixing lithium sintering. The precursor information prepared under certain conditions is shown in Figures S6 and S9.

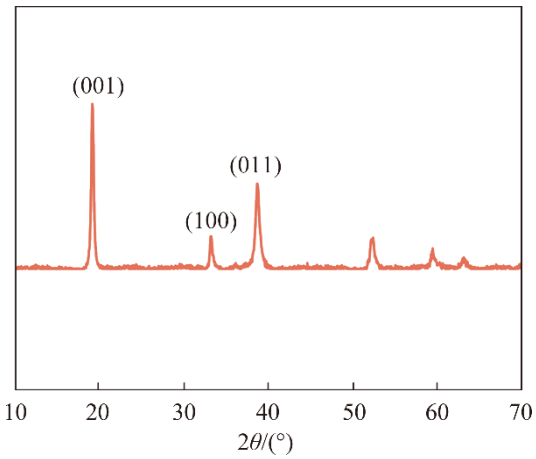

Figure S6 XRD pattern of NCM precursor

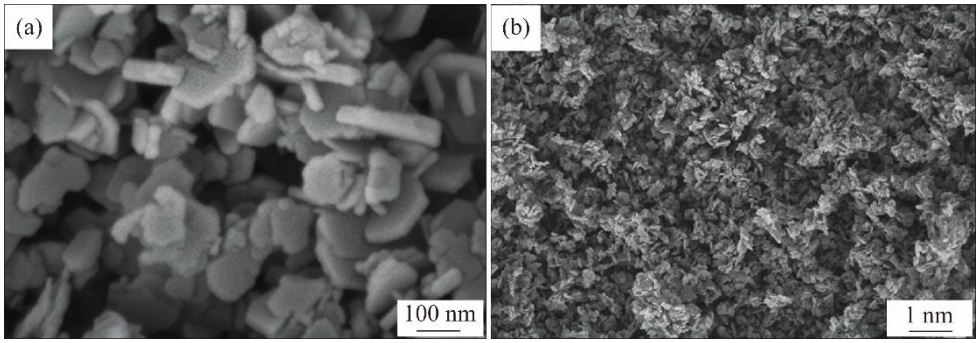

Figure S7 SEM images of NCM precursor

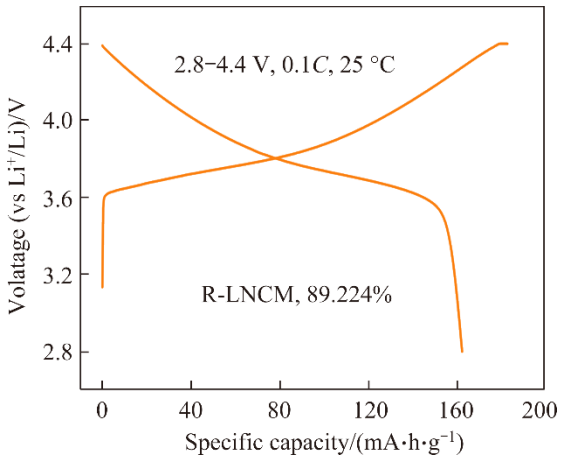

Figure S8 0.1*C* first cycle charge-discharge curve of R-LNCM

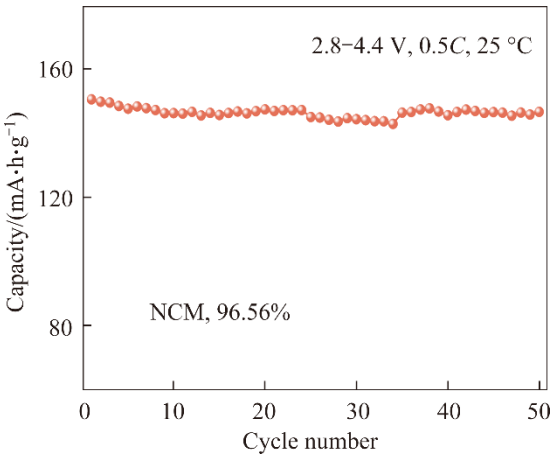

Figure S9 Cycle performance curve of R-LNCM at 0.5*C* in the voltage range of 2.8−4.4 V